How molecular internal-geometric parameters affect PB-PEO polymersome size in aqueous solution

Habel, Joachim Erich Otto; Ogbonna, Anayo; Larsen, Nanna; Schulte, Lars; Almdal, Kristoffer; Hélix-Nielsen, Claus

Published in:
Journal of Polymer Science. Part B, Polymer Physics

Link to article, DOI:
10.1002/polb.23954

Publication date:
2016

Document Version
Peer reviewed version

How molecular internal-geometric parameters affect PB-PEO polymersome size in aqueous solution

JOACHIM HABEL[1,2], ANAYO OGBONNA[2], NANNA LARSEN[3], LARS SCHULTE[4], KRISTOFFER ALMDAL[4], CLAUS HÉLIX-NIELSEN[1,2,5]

[1] Technical University of Denmark, Department of Environmental Engineering, Miljøvej, building 113, 2800 Kgs. Lyngby, Denmark

[2] Aquaporin A/S, Ole Maaløes Vej 3, 2200 Copenhagen, Denmark

[3] University of Copenhagen, Copenhagen Biocenter, Ole Maaløes Vej 5, 2200 Copenhagen, Denmark

[4] Technical University of Denmark, Department of Micro- and Nanotechnology, Produktionstorvet, building 423, 2800 Kgs. Lyngby

[5] University of Maribor, Laboratory for Water Biophysics and Membrane Processes, Faculty of Chemistry and Chemical Engineering, Smetanova ulica 17, 2000 Maribor, Slovenia

Dated: January 18, 2016

ABSTRACT: Amphiphilic polybutadiene polyethylene oxide (PB-PEO) is one of the best known chemistries to form stable vesicular morphologies, stated as polymersomes, in aqueous environment. Mimicking cell membranes, these structures self-assemble in an "amphiphilic window" determined by $0.15 < f < 0.35$ where f is the ratio between the hydrophilic block volume and the entire diblock volume. However the polymersome size distribution also depends on molecular weight (M_n) and in order to gain insight on how f and M_n together determine polymersome size, we prepared PB-PEO diblock copolymers with different block lengths and analyzed vesicle morphology via Dynamic light scattering (DLS) and Freeze-fracture transmission electron microscopy (FF-TEM). We found three main regimes: high f/low M_n with polymersomes of mixed diameter, high f/high M_n with mainly large polymersomes and low f, with mainly small polymersomes. In the first region, the polymersomes are highly polydisperse. There is a tendency towards increased diameter with increasing f and M_n. Taken together our findings can help to identify how polymersome self-assembly can be controlled to achieve size distribution specificity alleviating the need for subsequent tuning of size via extrusion. This can pave the way for cost-effective upscaling of polymersome production for biomedical and biomimetic applications.

Keywords: PB-PEO, Polymersomes, Self-assembly, Morphologies, Block copolymers

INTRODUCTION

Polymersomes are self-assembled vesicular (hollow spherical) systems based on amphiphilic block copolymers, where the copolymer contains two or more chemically distinct hydrophobic/hydrophilic monomer sequences that are covalently bonded. They are gaining interest due to their colloidal stability, versatile membrane properties and ability to encapsulate or integrate a broad range of drugs and molecules[1–5], as artificial cells[6–10] or matrix compartments for water channel proteins in biomimetic biomimetic membranes for water separation[11–16].

Self-assembly of polymers has been studied extensively theoretically[17–20] and experimentally[21–25]. Amphiphilic block copolymers can self-assemble into three main structural categories: bilayers, cylinders, and micelles depending on the interfacial curvature propensity. Thus bilayers form at low interfacial curvature propensity and with increasing interfacial curvature propensity, cylinders and micelles may form. There are two main mechanisms for polymersome formation, see Figure 1. One mechanism involves a closure of bilayer sheets resulting in vesicular shape and occurs when the energy loss due to surface tension is high enough that the vesicle shape is energetically preferable, see Figure 1 mechanism a[17]. Another mechanism involves nucleation (formation of semivesicles with a hydrophilic nucleus) with nucleus growth, see Figure 1 mechanism b[26]. In mechanism a at thermodynamic equilibrium, the polymersome size is related to a balance between the line tension γ, which is linearly related to the line energy E_{disk} of the bilayer sheet rim and the bending modulus κ, linearly related to the bending energy E_{bend} (Figure 1) where the polymersome diameter $d_P = \kappa/\gamma$[17].

For κ of 40 kT and γ of 1 kT, typical values for block copolymers[28], the theoretical mean d_P is 160 nm, which is in good agreement with reported experimental data[17]. However, based on experimental data, other factors than κ and γ can significantly influence polymersome size. These factors can be divided into four groups: internal-chemical factors (block chemistry, functionalization), internal-geometric factors (size, volume, number and distribution of each and both blocks), external-operational factors (conditions of preparation method) and external-environmental factors (temperature, composition and polarity of the solvent and additives). Table 1 lists some factors and their experimentally proven influences with main

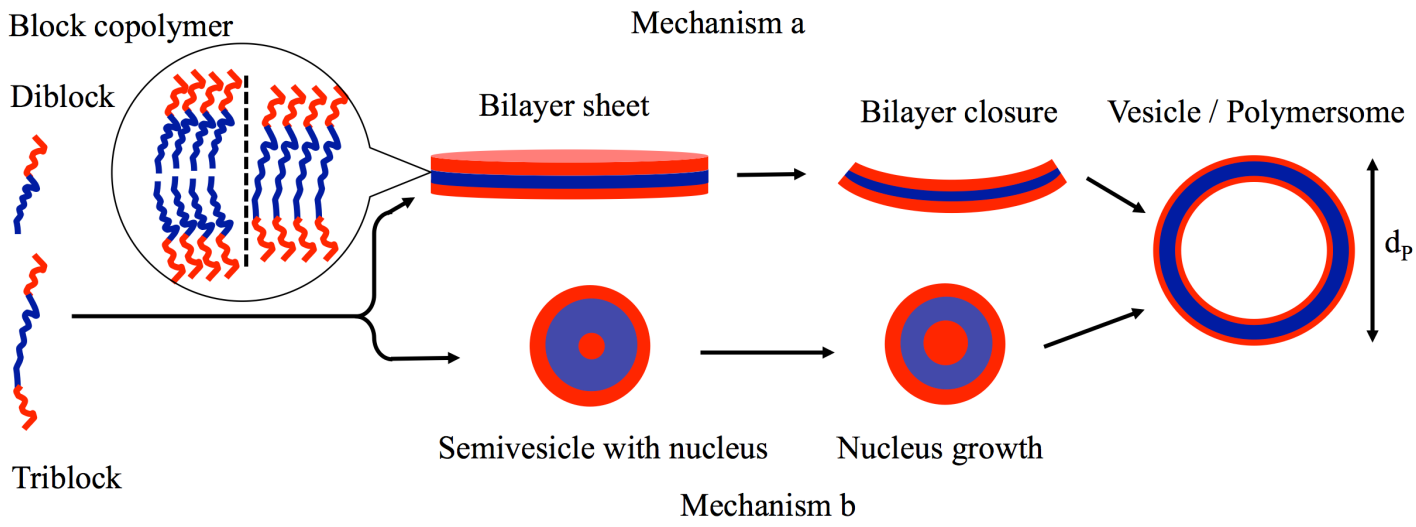

Figure 1: Sketch of forces behind polymersome formation at thermodynamic equilibrium[27]. Polymersomes can form due to a) bilayer closure to equilibrate out the line tension of the bilayer sheet rim γ and the bending modulus κ or b) to formation of a semivesicle with interior hydrophilic residues (nucleus) subsequent growth.

focus on internal factors.

Xiao and coworkers recently investigated theoretically, the internal-geometrical factors of polymersome self-assembly. Using dissipative particle dynamics (DPD) simulations of polymersomes formed by self-assembly of triblock copolymers, they modelled the polymersome size distribution with respect to the relationship of the polymersome bilayer thickness t_P and d_P at different f. At decreasing f, t_P dictates d_P to a higher extent, leading to a transition of large to small d_P[26].

Polybutadiene-polyethylene oxide (PB-PEO) represents a highly promising block copolymer chemistry due to its ability to form robust vesicles in aqueous solution[40–44] attributable to the low glass transition temperature of 1,2-polybutadiene (PB) of -10°C[45,46]. PB has a close relation to polyprenyl chains found in many animal and plant membranes[45]. PEO is the most commonly used biocompatible polymer, which is important in biomedical/biomimetic applications[46].

Most of the published experimental PB-PEO assembly studies focused mainly on the general morphology as a function of f[23,47–50]. The effect of M_n and f on PB-PEO polymersome

Table 1: Main factors influencing polymersome formation. For a given parameter (see abbreviation list for explanation) ↑ indicates an increase and ↓ a decrease.

Polymer chemistry	Size range [nm]	Influencing factor	Factor change	→ Response change	References
PS-PAA	100-500	f_{mol}	f_{mol} ↑	→ d_P ↓	[29]
PEE-PEO	N/A	M_n	M_n ↑	→ Stability ↑	[30]
PGC	150-550	M_w	M_w ↑	→ d_P ↑	[31]
PEE-PEO	∼40000	M_w	M_w ↑	→ Fluidity ↓	[32]
PDMS-PMOXA	∼20000	$M_{n,PDMS}$	$M_{n,PDMS}$ ↑	→ D_L ↓	[33]
PDMS-PMOXA	20-150	$M_{n,PDMS}, f_w$	$M_{n,PDMS}$ ↑, f_w ↓	→ d_P ↑	[34]
PS-PAA	30-90	$PDI_{MM,PAA}$	$PDI_{MM,PAA}$ ↑	→ d_P ↓	[35,36]
PMPC-PDPA	50-350	T	T ↑	→ d_P ↓	[37]
PS-PAA	50-100	$c_{P,wt}$	$c_{P,wt}$ ↑	→ d_P ↑	[38]
PS-PAA	100-500	Additives	NaCl, HCl ↑, NaOH ↓	→ d_P ↓	[29]
PEE-PEO	∼25000	Surfactants	Surfactant	→ Stability ↓	[39]

bilayer thickness[51], mechanistic properties[46], detergent response[52], mixtures of two PB-PEO polymers[53] or adhesiveness of functionalized PB-PEO polymersomes[54] have also been investigated. However, to our knowledge, no systematic size-distribution study exists for PB-PEO polymersomes, therefore this study focuses on the combined effect of M_n and f on d_P based on PB-PEO polymersome formation in aqueous solution. In this study, d_P and polydispersity of d_P will be determined by using DLS and FF-TEM. For DLS analysis, polydispersity index (PDI_{DLS}) is quantified as the ratio:

$$PDI_{DLS} = \frac{\delta^2}{Z_D^2} \tag{1}$$

where δ is the distribution width of d_P and Z_D the intensity-weighted hydrodynamic d_P, obtained by DLS cumulant analysis[55]. A related measure of the polydispersity is the variation coefficient:

$$V_{DLS} = \frac{\delta}{\langle d_P \rangle} \tag{2}$$

where $\langle d_P \rangle$ is the mean value of d_P. For analysis using FF-TEM, polydispersity is quantified as:

$$\sigma = \sqrt{\sum_{i=1}^{n} (d_{p(i)} - \langle d_P \rangle)^2} \tag{3}$$

where σ is the standard deviation of the manual d_P measurements from a total of n polymersomes. The FF-TEM derived variation coefficient is defined as:

$$V_{FF-TEM} = \frac{\sigma}{\langle d_P \rangle} \tag{4}$$

This knowledge can be very helpful in controlling the polymersome particle size and distribution and thereby circumvent the expensive and time-consuming extrusion process normally employed during production and scale-up of polymersomes for pharmaceutical, biomedical and biomimetic applications.

EXPERIMENTS

Polymer synthesis via one-step approach

All diblock copolymers except PB_{43}-PEO_{32} and PB_{74}-PEO_{60} were synthesized via one-step ring-opening anionic polymerization according to Förster[56]. Here, butadiene (Bd) and ethylene oxide (EO) monomers were purified and dried via cooling with liquid nitrogen and distilled over *n*-dibutylmagnesium (*n*-Bu_2Mg) and *n*-butyl lithium (*n*-BuLi) to remove traces of impurities. The synthesis solvent Tetrahydrofuran (THF) was purified and dried via reflux and stirred over sodium in benzophenone and paraffin.

For polymerization of Bd, THF was first introduced in a predried reactor and cooled to -40°C. Bd was added, followed by *n*-BuLi. The reaction was allowed to run for 4h at -20°C, where the polybutadienyl lithium appeared in a yellow or orange colour. This step was followed by cooling down the mixture to -40°C and approximately 1ml of EO was added to stop the polymerization, visibly by the disappearance of the yellow colour. The following reaction was left for 1.5 h at -40°C. A precursor was drawn and analysed via size exclusion chromatography (SEC) on a SIL-10AD (Shimadzu, Kyoto, Japan). The SEC system consisted of a Shimadzu LC-10AD High performance liquid chromatography (HPLC) pump together with a Viscotek Differential Refractometer model 200 differential refractometer followed by the columns 5cm Polymer Laboratories, Guard column 3mm, 30x7.8cm Waters Styragel HMW 6E, and 30x7.5cm Polymer Laboratories, PLgel 5 mm Mixed-D. The columns were kept at room temperature during the measurements. Non-stabilized THF was used as eluent, and the system was calibrated using polystyrene standard samples having very narrow molar mass distributions.

For EO polymerization, remaining EO was added followed by injection of 1-*tert*-Butyl-4,4,4-tris(dimethylamino)-2,2-bis[tris(dimethylamino)-phosphor-anylidenamino]-2λ^5,4λ^5-catenadi-(phosphazene) (tBuP4) in a molar *n*-BuLi-tBuP4 ratio of 1:1 to ensure exact stoichiometry[56]. This step was followed by heating the reaction to 40°C to start EO chain propagation. Two days later, the reaction was quenched with acetic acid. The polymer was precipitated in cold acetone followed by vacuum drying. Bd-EO stoichiometry was analyzed by nuclear magnetic resonance (NMR) at 300 or 400 MHz. The polydispersity index of the raw polymer (PDI_M) was analyzed via SEC. Further details can be found in the supplementary information. The polymer was stored at -20°C until use. All synthesized polymers are list in table 2.

Polymer synthesis via two-step approach

PB_{43}-PEO_{32} and PB_{74}-PEO_{60} were synthesized following a two-step-approach by[57]. The Bd was polymerized as mentioned above followed by direct precipitation in cold acetone. This step was followed by vacuum drying of PB that was following an introduction in a predried reactor together with purified THF. This step was followed by titration with potassium naphthalenide into the solution until a slight green color remained for at least 30 min. EO was added and the reaction was allowed to heat to 45°C run for 20 h. The following termination was done with acetic acid. Precipitation, analysis and storage was done like described above.

Polymersome formation

For polymer stock solutions, 100 mg was thawed, weighed and dissolved in 10 ml $CHCl_3$ in order to get a 10 mg/ml solution. This step was followed by a sonication for 5min. Storage was at -20°C until use. 2.5 ml of the stock solution was injected in a 5 ml round flask, followed by evaporating the $CHCl_3$ on a rotary evaporator for at least 2 h at room temperature and 2 mbar at a rotation speed of 125 rpm until the polymer remained as a smooth film on the flask wall. This step was followed by a rehydration of the sample with 200 μl of tris buffer (10mM tris pH 8.0, 50mM NaCl) with 1,3% *n*-octyl-β-D-glucoside (OG) to facilitate the release of the film, and the sample was left stirring overnight at 4°C. The sample was diluted with 800 μl tris buffer, followed by addition of 20mg biobeads (Bio-Rad, Hercules, USA) to remove the OG between the polymersome bilayer. The sample was

Table 2: Overview table of all synthesized polymers with M_n (calculated from ^{1}H NMR analysis), PDI_M (based on size-exclusion chromatography (SEC) analysis with polystyrene standard calibration) and the hydrophilic volume fraction f. PB_{43}-PEO_{32}. PB_{74}-PEO_{60} and PB_{107}-PEO_{22} were synthesized with a different synthesis method[57] than the other polymers, starting with the EO-endcapped PB. Calculation of f is given in the supplementary information

Polymer	M_n **[kg/mol]**	PDI_M	f
PB_{29}-PEO_{16}	2.3	1.076	0.258
PB_{29}-PEO_{19}	2.4	1.086	0.294
PB_{33}-PEO_{18}	2.6	1.087	0.251
PB_{47}-PEO_{7}	2.8	1.109	0.089
PB_{32}-PEO_{30}	3.0	1.094	0.367
PB_{45}-PEO_{14}	3.0	1.078	0.161
PB_{43}-PEO_{32}	3.8	1.110	0.316
PB_{46}-PEO_{32}	3.9	1.080	0.301
PB_{60}-PEO_{25}	4.3	1.080	0.207
PB_{62}-PEO_{56}	5.8	1.081	0.356
PB_{74}-PEO_{60}	6.7	1.081	0.333
PB_{104}-PEO_{31}	7.0	1.244	0.155
PB_{121}-PEO_{25}	7.7	1.092	0.111
PB_{120}-PEO_{41}	8.3	1.072	0.175
PB_{92}-PEO_{78}	8.4	1.167	0.344
PB_{104}-PEO_{77}	9.0	1.130	0.314
PB_{117}-PEO_{61}	9.1	1.204	0.245

left on a shaker with 200 rpm for 3 h at room temperature (RT), followed by addition of another 20 mg of biobeads. The sample was then left overnight shaking with 200 rpm at 4°C.

Analysis of d_P via freeze fracture and transmission electron microscopy (FF-TEM)

FF was performed on a MED020 with EM VCT100 shuttle attached (Leica, Wetzlar, Germany). 1.2 μl sample was injected into a 3 mm aluminium sample carrier at the side with 300 μm depth and covered with another aluminium plate of 200 μm depth side, care was

taken to avoid air bubbles in between. This sandwich was plunged into liquid ethane for 20 s, followed by immediate plunging in liquid N_2. The sample carrier was fixed at the sample holder, followed by introduction in a high vacuum chamber at -140°C. This step was followed by removal of the lower sample carrier, where sample coating was following at the same temperature with 2 nm carbon, followed by 4 nm platinum tilted at 45° and finally with a 19nm carbon protection layer without tilt. Outside of the chamber, the carrier was thawed for 5 min at RT, followed by carefully replacement in 45° into a 200 μl bath of tris buffer with 10%OG for 5 min for solubilizing the polymersomes. The final step was to place an uncoated TEM copper grid with 400 Mesh at 45° below the replica or single pieces of it. TEM observation was done with a CM100 (Philips, Amsterdam, Netherlands) with an installed Veleta 2k CCD camera (Olympus, Shinjuku, Japan). On a tungsten source, the applied voltage was 80 kV with a 100 μm objective lense aperture. Analysis of d_P on the TEM images was done by manual measurement (after semi-automatic measurement using ImageJ with various plugins failed to work due to too low contrast between polymersomes and background) using the image software Gimp, followed by multiplication of all values with a correction factor of $4/\pi$[58].

Analyis of d_P via DLS

DLS was done with a Nano Zetasizer (Malvern, Worcestershire, UK). 800 μl sample were injected in a disposable cuvette, followed by three measurements with 6 runs of 10 s per measurement at RT. Raw data of autocorrelation functions of PB_{33}-PEO_{18}, PB_{46}-PEO_{32} and PB_{92}-PEO_{78} as examples can be found in the supplementary information.

RESULTS AND DISCUSSION

Stable PB-PEO based polymers with M_n ranging from 2.3 – 9.1 kg/mol and f between 0.089 – 0.367 were synthesized as shown in Table 2. Utilizing the film rehydration technique, polymersomes were formulated with the synthesized polymers and characterized using DLS and FF-TEM. First sample preparation will be discussed, in terms of how it can be adopted to ensure minimal external influence on d_P, how the analytical methods used (DLS and

FF-TEM) can influence d_P and how one may minimize such influence. Then, results will be compared from DLS and FF-TEM as well as their compatibility or correlation of data generated from them. Finally, the influence of M_n on d_P, the influence of f on d_P and the combined effect on d_P of changing both M_n and f will be discussed.

Issues in experimental determination of polymersome diameter

Influence of sample preparation

During polymersome preparation and analysis, commonly used techniques including centrifugation, dilution and agitation can affect their formation, quality and stability[59]. It is therefore necessary to minimize these external influences as much as possible. In the present study, we prepared all polymersomes with no dilution, centrifugation and minimal agitation during preparation and analysis. To ensure reproducibility, three sample sets are prepared per polymer. Most samples exhibited high turbidity (polymer concentration: 25 mg/ml) throughout the preparation.

Influence of DLS algorithms

It is well-known that DLS is biased towards larger particles, because they scatter light more strongly. To minimize this bias, volume size distribution is used instead of the intensity size distribution. The latter is based on Rayleigh scattering that has a intensity-particle-diameter-relationship $I \sim d^6$, where the former is based on Mie scattering that compensates for the strong dependency[60]. Another problem is the polydispersity of samples. The DLS instrument uses two algorithms to measure particle sizes: cumulant analysis and non-negatively constrained least squares (NNLS). Cumulant analysis is more convenient to use, however it assumes only a single particle family (e.g. spheres with narrow size distribution) and is thus not suitable for polydisperse samples. In DLS analysis, polydispersity is quantified as PDI_{DLS} (Equation 1). From previous experiments, we know that the studied polymersomes have a higher PDI_{DLS} than 0.25[21], where cumulant analysis is not recommended to use[55]. Thus, all values are extracted from the NNLS analysis. NNLS generally introduces several algorithm operators to extract information from the autocorrelation curve generated by DLS. Thus, micelles, different polymersome classes or aggregates can be easier differenti-

ated[61]. Another issue is the unusually high polymersome concentration (25 mg/ml) leading to high turbidity. The DLS instrument can however compensate highly turbid samples using non-invasive back scattering (NIBS) at 173° detection angle. Thus, laser attenuation as well as measurement position in the cuvette can be adjusted to sample turbidity[62–64]. However, a potential error source could arise due to strong scattering of highly turbid samples. However, to compare FF-TEM and DLS properly (and minimize influences of external factors) both need to be performed at the same concentration. Lower polymer sample concentrations would however lead to high levels of bad fracturing. We therefore decided to keep 25 mg/ml as fixed concentration throughout all experiments.

Influence of FF-TEM on d_P

FF reveals information about polymersome size as the original shape in aqueous solution is preserved by changing the aggregate state of the solution to the glassy state during quick-freezing without the formation of ice crystals. Compared to negative-staining TEM, there is no labeling with heavy metal derivates that could cause deformation and/or osmotic shrinkage of the polymersomes. Additionally, one can obtain a more 3D-like appearance in contrast to Cryo-TEM. The major drawback is that the polymersomes are not all fractured in the equatorial plane, meaning that the observed diameter is often smaller than d_P. Although we apply a correction factor $(4/\pi)$[58], the difference between observed and real diameter remains a source of error for FF-TEM. The advantage of working with the planchet technique (details in the Material & Methods section) is that the smearing effects are minimized, however not completely removed. As the observed $\langle d_P \rangle$ is larger than the diameter of PB-PEO micellar structures (15-40nm[49]) and from former Cryo-TEM observations on PB_{29}-PEO_{16}[65] we conclude that the majority of spherical structures observed are polymersomes. For the PB-PEO diblock copolymers investigated, FF-TEM revealed highly polydisperse samples that were spread over the whole replica (Figure 2a), distributed in small islands between non-fractured polymersome-free planes (e) or in river-like arrangements (c). All these samples had well-defined edges and clear three-dimensional appearance. Other samples had well-defined edges as well but appeared more planar (Figure 2f).

The difference between Figure 2a, g and c could be due to the fact that each polymersome

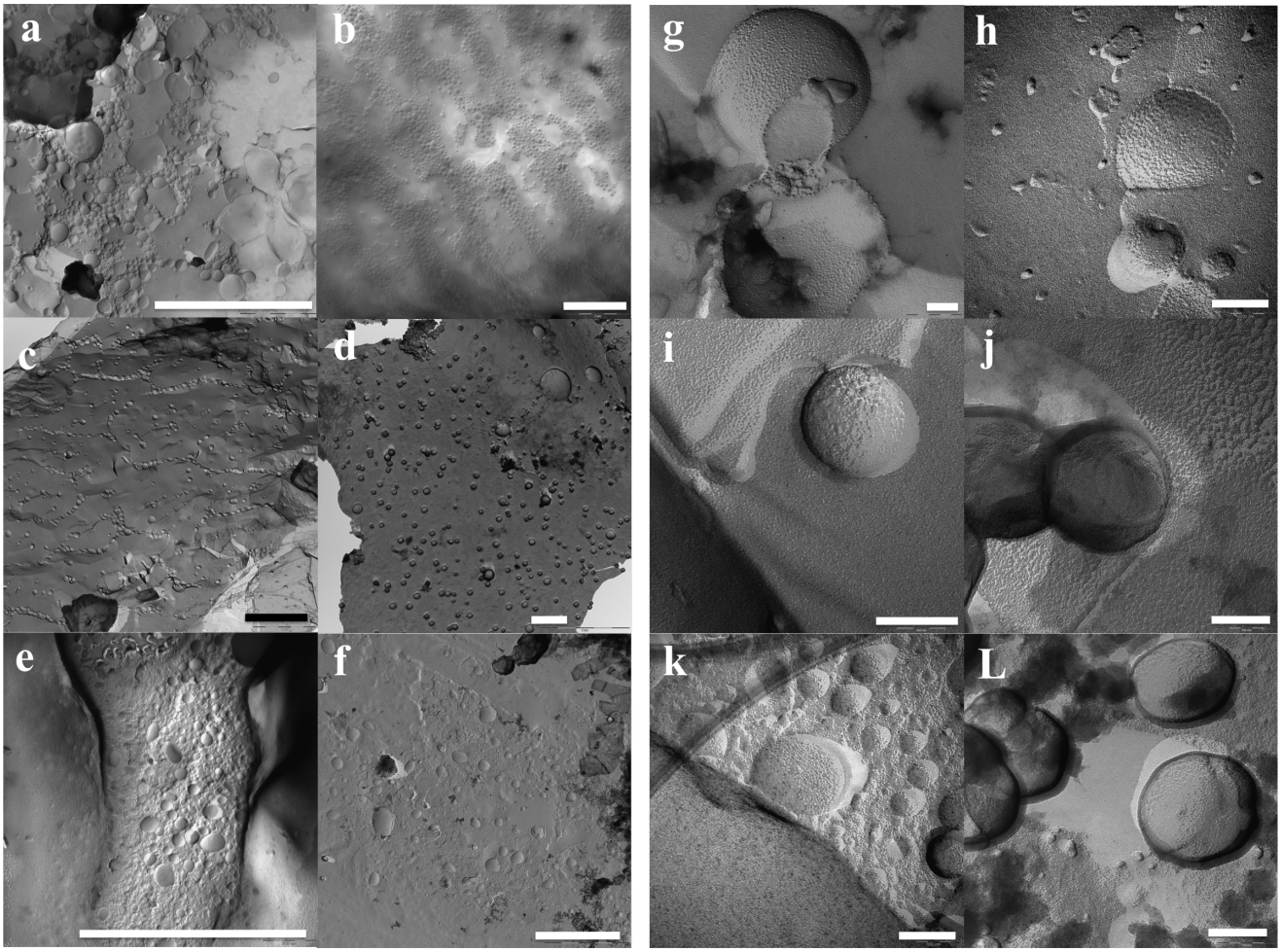

Figure 2: FF-TEM micrographs of PB-PEO polymersomes of different M_n and f, sorted after increasing M_n. a)+g) PB_{29}-PEO_{16}, c)+i) PB_{29}-PEO_{19}, e)+k) PB_{33}-PEO_{18}, b) PB_{60}-PEO_{25}, h) PB_{45}-PEO_{15}, d)+j) PB_{74}-PEO_{60}, f)+L) PB_{92}-PEO_{78}. Scale bar is 1 μm for a-f and 100 nm for b-L. Polymersomes were spread over larger areas (a), islands (e) or river-like arrangements (c), where they exhibited well-defined edges. At fragile areas of the ends of the replica, the displacement of polymersomes left black rings on the edges (d) complicating the measurement of their d_P. Few samples exhibited a more flat (f) or shallow appearance (b), the last is probably not fractured. When observing at higher magnification, all polymersomes had rougher (i+h) or finer (g+k) grains on their surface. The white shadow is generated during platinum shadowing at 45°.

population was at a different position inside the planchet and the presence of air bubbles in the planchet. The possible solution turbulence involved in the vitrification process was probably higher at the edges of the planchet, forcing the polymersomes to accumulate around turbulent areas in the observed river-like arrangements in Figure 2c. The turbulence forces had a less pronounced effect on larger polymersomes consistent with the observation that there were seldom micrometer size polymersomes present in the river-like arrangements. The "islands", observed in Figure 2e, could be due to air bubbles, creating solution-free gaps between both planchets. However, all these factors are not influencing d_P determination *per se*. A few polymersome samples had less well-defined edges and generally exhibited a more shallow appearance (Figure 2b). These polymersomes were probably not fractured but could be facing the air-water-interface of a captured air bubble. Here, no correction factor would apply as far as no fracture occurred. We rarely observed these structures, thus we assume their influence on d_P to be negligibly small.

Many samples showed black rings around the polymersomes (Figure 2d, j + L). The black-ring polymersomes are probably located at fragile areas at the edges of the replica. Displacement of the original polymersomes will result in low resolution of the most fragile parts of the replica (the polymersome edges) and the thickness of the black ring will affect the precision of d_P determination[66]. The manual measurement was performed from the outer (well-defined) edge of the black ring to ensure reproducible d_P readings. At higher magnification, polymersomes appeared in raspberry-like spherical shapes covered with grains, sometimes revealing an opened inner bilayer (see Figure 2j) or a shadow from the 45° platinum coating (Figure 2i, h and k). Chambon and coworkers observed similar structures of polyglycerol monomethacrylate-polyhydroxypropyl methacrylate-polybenzyl methacrylate (PGMA-PHPMA-PBzMA) triblock copolymers[67]. To avoid any artifacts, d_P measurements are taken at the side without shadow. Due to bad fracturing, there could be small dots at the polymersome edges (see Figure 2h). However this has only a negligible effect on d_P determination. For each of the triplicates, a minimum of 100 polymersomes is measured, resulting in a minimum of 300 polymersomes per polymer. FF-TEM revealed d_P between 100 nm and 300 nm, where σ was often larger than d_P resulting in $V_{FF-TEM} > 1$ (Equation 4).

FF-TEM can be biased towards larger polymersomes as well, because these are the ones that

can be observed easiest when screening the TEM grid. So even if there is only one large polymersomes out of 1000 polymersomes, there is a strong bias towards it if there are only 100 polymersomes analyzed per batch. On the other hand it can also lead to false results if they are left out of the analysis even though they have been observed. To overcome this problem, it would require manual measurement of 1000 or more polymersomes per batch, which is beyond the scope of this study. However based on the work of Terreau and coworkers[36] we are confident that our sampling is sufficient to assess $\langle d_P \rangle$.

Issues in comparing from DLS versus FF-TEM

All spherical self-assembled morphologies from a FF-TEM image are measured in terms of d_P, regardless if they could be micelles or polymersomes. To be able to compare DLS and FF-TEM, the multi-peak distribution from the DLS NNLS analysis was normalized into one effective peak by performing a weighted average. Comparing the normalized $\langle d_P \rangle$ vales from DLS analysis with values from FF-TEM, $\langle d_P \rangle$ values from the DLS analysis were on average 64±39% higher than values from the FF-TEM analysis. The largest difference was 83.7% for PB_{29}-PEO_{19}, the smallest difference 39.5 for PB_{46}-PEO_{32}. Even when using volume size distribution, DLS is still highly biased towards larger particles. The $\langle d_P \rangle$ difference between DLS and FF-TEM can thus be to the presence of large aggregates appearing as one particle in DLS analysis, whereas they are left out in FF-TEM analysis. Terrau et al. compared DLS and TEM measurements and also obtained larger $\langle d_P \rangle$ with DLS than with TEM, which they explained by the appearance of aggregates[36]. The maximal d_P values which we could determine reliably from FF-TEM images were around 1.5μm. Thus effectively all structures larger than this are excluded in the manual FF-TEM analysis of the d_P distribution. We therefore also omitted all morphologies with an apparent $d_P > 1.5$ μm from the DLS analysis corresponding to less than 15% of the total mass content. After this correction, the difference in $\langle d_P \rangle$ went down to 38±22%, where the highest difference was 75.8% observed for PB_{46}-PEO_{32}) and the smallest was only different by 5.4% for PB_{60}-PEO_{25}, for details see supplementary information. A general tendency is that $\langle d_P \rangle$ values of polymersomes with $V_{FF-TEM} > 0.9$ are 50% larger in DLS analysis compared to FF-TEM. We believe that these corrections (normalization and exclusion of large structures) are sufficient to enable a

comparison of DLS and FF-TEM, although we cannot fully exclude that some of the larger d_P values captured by DLS in fact represent aggregates rather than polymersomes.

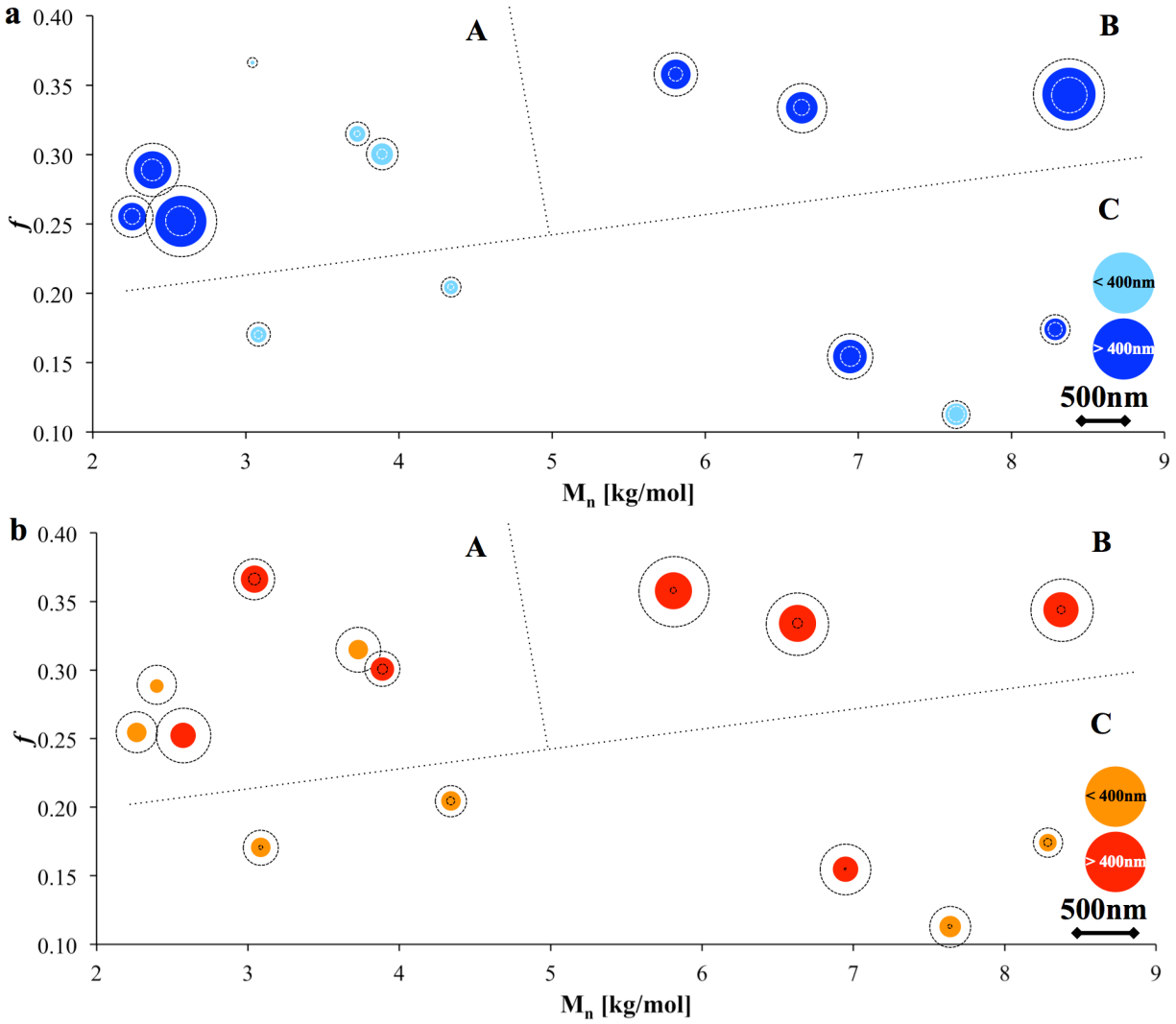

Figure 3: Visualization map of the effect of M_n and f on d_P from DLS (a) and FF-TEM (b). $\langle d_P \rangle$ is indicated as full circles (blue and red/orange for DLS and FF-TEM respectively) and the concentric dotted circles indicate $\langle d_P \rangle \pm \delta$ for DLS and $\langle d_P \rangle \pm \sigma$ for FF-TEM. If $\langle d_P \rangle < 400$ nm in (a), the circle color is changed to bright blue in and if $\langle d_P \rangle < 150$nm in (b), the circle color is change to bright red. Three regions are indicated: a region with mixed high/medium/low d_P values (labeled A), a region with medium/high d_P values (labeled B) and a region with medium/low d_P values (labeled C).

The relation between d_P and M_n & f

We now analyze how d_P depends on M_n and f. The relationship is depicted in Figure 3 where Figure 3a show data from the DLS measurements. $\langle d_P \rangle$ is indicated as full circles (blue and red for DLS and FF-TEM respectively) and the concentric dotted circles indicate $\langle d_P \rangle \pm \delta$ for DLS and $\langle d_P \rangle \pm \sigma$ for FF-TEM. Although the d_P distribution seems to scatter considerably in the (M_n,f) parameter space we can identify three regions: a region with mixed high/medium/low d_P values (labeled A), a region with medium/high d_P values (labeled B) and a region with medium/low d_P values (labeled C). Our finding are on contrast to the findings of Wu et al. who observed a decrease d_P with increasing f for PDMS-PMOXA diblock copolymers[34]. Hypothetically, this difference could be due to steric repulsion of PMOXA, which may be less pronounced for PEO, as far as the oxazoline ring of PMOXA has a higher steric effect than the PEO monomer.

From the FF-TEM analysis, there was a slight increase in d_P with higher M_n for $f > 0.2$. Bermudez et al. reported an increase in t_P with increasing M_n[51] for PB-PEO polymersomes. From M_n of 3.6 to 5.2 kg/mol, they observed an t_P increase of 1 nm (9.6 to 10.6 nm). Doubling the M_n resulted in an increase in t_P of one third (M_n 10.4 and 20 kg/mol resulted in a t_P of 14.8 and 21 nm respectively). Additionally, Ma et al. reported a linear dependence between t_P and d_P for three out of four polymersomes[68]. Combining these results a linear relationship between t_P/M_n and t_P/d_P could substantiate the findings of an increased d_P with increasing M_n. However the study of Ma et al. was made on PS-PAA polymersomes with M_n between 25 and 55 kg/mol, which complicates a direct comparison. Experimental studies on PS-PAA are generally performed in a mixture of water and organic solvent. This is not the case here where we analyzed PB-PEO with water as the sole solvent. As far as PS is less soluble in water than PB, PS-PAA cannot be made by film rehydration but need to be brought into the aqueous phase by slow solvent exchange[68,29]. Thus, the external-environmental factors fundamentally different for PS-PAA compared to PB-PEO which makes a direct comparison difficult.

For both DLS and FF-TEM there is a tendency for $\langle d_P \rangle$ to increase with increasing f (see f vs d_P in the supplementary information). For $f < 0.2$, $\langle d_P \rangle$ was between 100-200 nm,

irrespective of M_n. For $f > 0.2$, some $\langle d_P \rangle$ increased up to 200-300 nm but with considerable variation as function of M_n. The increase is more pronounced in Figure 3b than in Figure 3a, probably to the issues in obtaining $\langle d_P \rangle$ values from polydisperse samples with DLS. The increase is in agreement with the DPD simulations of Xiao et al. who reported an increase in $\langle d_P \rangle$ with increasing f[26]. They explained this phenomenon with expansion of the hydrophilic blocks in order to maximize the contact with the solvent. The expansion is stronger with increasing f so that larger polymersomes would exhibit more hydrophilic blocks in expanded conformation[26]. On the contrary, Choucair et al. found a decreasing d_P with increasing f on PS-PAA polymersomes[29]. A comparison is hampered by the fundamental differences between PS-PAA and PB-PEO as discussed before.

For $0.17 < f < 0.2$, δ was minimal with DLS and σ was also low with FF-TEM for the polymersomes of PB_{45}-PEO_{15} (M_n =3.1 kg/mol), PB_{60}-PEO_{25} (M_n0 = 4.3 kg/mol) and PB_{120}-PEO_{41} (M_n = 8.3 kg/mol). Xiao et al. concluded similarly a minimal PDI with long hydrophobic chain length[26]. They ascribed this to a minimization of energetically unfavorable interactions between the hydrophobic chains and the aqueous solution thus no shielding of the hydrophilic segments was necessary. Ma et al. also experimentally reported an increased PDI with increasing hydrophilic block length[68], but with PS-PAA polymersomes.

From a thermodynamical point of view, we assume mechanism a from the introduction as the major mechanism since mechanism b applies to more hydrophobic polymers like PDMS[26,69]. Thus, it may be that in regions B and C in the (M_n,f) parameter space (Figure 3), the equilibrium between E_{disk} the driving force to keep the bilayer structure open and E_{bend}, the driving force to close the bilayer to vesicular structure, is one broad energetic minimum. For polymers in region B (M_n 5-9 kg/mol and f 0.2-0.4), as well as for polymers in region C (M_n 3-9 kg/mol and f of 0.1-0.2), the bilayer closure or nucleation growth results therefore in one dominant d_P. Thus, polymersomes in these regions had less polydispersity than in region A (M_n 2-5 kg/mol and f 0.2-0.4). Here, the energy difference behind bilayer closure/nucleation growth is smaller which likely results in several energetic minima, leading to d_P variation and higher polydispersity.

In order to obtain more insight into how the polydispersity may depend on the characterization method, we analyzed how the variation coefficients V_{DLS} and V_{FF-TEM} depend on M_n

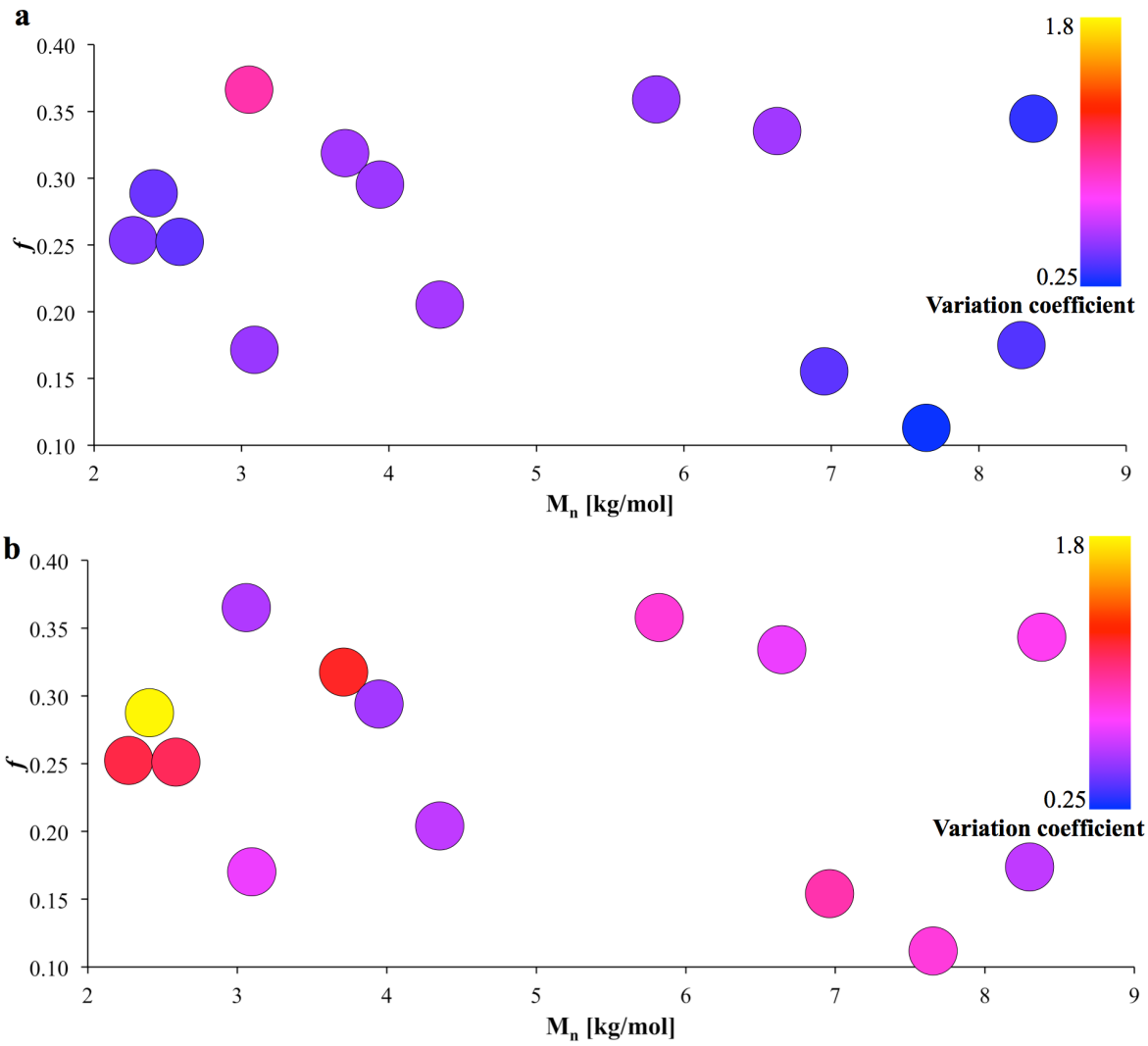

Figure 4: Variation coefficients as function of M_n and f for DLS and FF-TEM analysis. (a) V_{DLS} calculated using Equation 2. (b) V_{FF-TEM} calculated using Equation 4. The color changes from blue to red to yellow with increasing variation coefficient. The regions A, B and C from Figure 3 are also reflected in this map. The variation coefficients are rather low in region B and C, where the are increased and different in region A. The effect is more pronounced for V_{FF-TEM}.

and f, shown in Figure 4. V_{DLS} is 45±22% lower than V_{FF-TEM} (excluding PB_{32}-PEO_{30} with the reverse ratio mentioned before). In region B and C, V_{DLS} and V_{FF-TEM} are low, consistent with the obtained δ and σ values, see Figure 3. In region A, the variation coefficients were more different, where the difference between V_{FF-TEM} was higher than in

the case of V_{DLS}. The underlying weak energy function in region C is also reflected in the variation coefficients. The resulting randomly d_Ps are especially visible in the different V_{FF-TEM}s of PB_{43}-PEO_{32} and PB_{46}-PEO_{32} that have a difference in M_n and f of only 0.1 kg/mol and 0.02 respectively. Xiao revealed as well that samples with lower f assemble to more monodisperse samples[26].

CONCLUSIONS

In conclusion, polymersomes based on PB-PEO were prepared under identical conditions and analysed via DLS and FF-TEM to determine how $\langle d_P \rangle$ depends on M_n and f. Both methods of analysis revealed highly polydisperse samples. We defined three main regions in the (M_n,f) parameter space: A (high f/low M_n) with mixed high/medium/low d_P and high polydispersity, B (high f/high M_n) with high/medium d_P and medium polydispersity and C (low f) with low/medium d_P and medium polydispersity. There is a tendency towards increased diameter with increasing f and M_n. These observations are a first step into the complex and sensitive interplay between block length and morphology at the "amphiphilic window" between f 0.15 and 0.35 where polymersomes are forming. The understanding of underlying mechanism enables the chemical fine-tuning to achieve desired size distributions for the use of polymersomes as nanoreactors, drug delivery system or matrix compartment for biomimetic membranes.

ACKNOWLEDGMENTS

We thank Daniela Pirner, University of Bayreuth, Germany, and Sokol Ndoni, DTU Nanotech, for helpful discussions and Simon Levinsen, DTU Nanotech for assistance in polymer synthesis; Fabian Itel and Mohamed Chami, both University of Basel, Switzerland, and Manish Kumar, Pennsylvania State University, USA, for useful discussions about polymersomes in general and freeze fracture; Fadoua Sbai, Aquaporin A/S for assistance with polymersome preparation; Klaus Qvortrup and Ramon Liebrechts, University of Copenhagen, for providing assistance with freeze fracture and access to the Leica freeze fracture instruments. JH was supported by an industrial PhD grant from Innovation Fund Denmark.

CHN was supported by the IBISS - Industrial Biomimetic Sensing and separation platform (http://www.ibiss.dtu.dk) funded by the Danish Innovation Fund Grant no. 097-2012-4.

ABBREVIATIONS / NOMENCLATURE

Bd - 1,3-Butadiene

n-BuLi - *n*-Butyl lithium

n-Bu_2Mg - *n*-Dibutylmagnesium

$c_{P,wt}$ - Polymer weight concentration

d_P - Polymersome diameter [nm]

$\langle d_P \rangle$ - Mean d_P

PDI_M - Polydispersity index of the polymer length, defined as M_w/M_n

D_L - Lateral diffusion coefficient [$\mu m^2/s$]

DLS - Dynamic light scattering

E_{bend} - Bending energy of vesicle

E_{disk} - Line energy of vesicle bilayer sheet rim

EO - Ethylene oxide

f - Hydrophilic volume ratio

f_{mol} - Hydrophilic molar ratio

f_w - Hydrophilic weight ratio

HPLC - High performance liquid chromatography

M_n - Number averaged molecular weight

M_w - Weight averaged molecular weight

NIBS - Non-invasive back scattering

NMR - Nuclear magnetic resonance

NNLS - Non-negatively constrained least squares

OG - *n*-octyl-β-D-glucopyranoside

PAA - Polyacrylic acid

PB - 1,2-Polybutadiene

PBzMA - Polybenzyl methacrylate

PDI_{DLS} - Polydispersity index of d_P by DLS analysis

PDMS - Polydimethylsiloxane

PDPA - Polydiisopropylaminoethyl methacrylate

PEE - Polyethylethylene

PEO - Polyethyleneoxide

PGC - Palmitoyl glycol chitosan

PGMA - Polyglycerol monomethacrylate

PHPMA - Polyhydroxypropyl methacrylate

PMOXA - Polymethyloxazoline

PMPC - Polymethacryl oyloxyethylphosphorylcholine

PS - Polystyrene

SEC - Size exclusion chromatography

t_P - Polymersome bilayer thickness [nm]

tBuP4 - 1-*tert*-Butyl-4,4,4-tris(dimethylamino)-2,2-bis[tris(dimethyl-amino)-phosphoranylidenamino]-$2\lambda^5$,$4\lambda^5$-catenadi(phosphazene)

TEM - Transmission electron microscopy

THF - Tetrahydrofuran

V_{DLS} - Variation coefficient of DLS analysis

V_{FF-TEM} - Variation coefficient of FF-TEM

Z_D - Intensity-weighted hydrodynamic d_P

δ - Distribution width of d_P measured with DLS

γ - Line tension of polymersome bilayer sheet rim

κ - Bending modulus of polymersome

σ - Standard deviation of FF-TEM d_P measurements

References

1. J. Nicolas, S. Mura, D. Brambilla, N. Mackiewicz, and P. Couvreur, Chem. Soc. Rev. **42**, 1147 (2013).

2. J. Yang, H. Liu, and X. Zhang, Biotechnol. Adv. **32**, 804 (2014).

3. K. Langowska, C. G. Palivan, and W. P. Meier, Chem. Commun. **49**, 128 (2013).

4. P. V. Pawar, S. V. Gohil, J. P. Jain, and N. Kumar, Polym. Chem. **4**, 3160 (2013).

5. R. Langer, Science **249**, 1527 (1990).

6. S. Egli, M. Nussbaumer, V. Balasubramanian, M. Chami, N. Bruns, C. G. Palivan, and W. P. Meier, J. Am. Chem. Soc **133**, 4476 (2011).

7. L. Kuang, D. A. Fernandes, M. O'Halloran, W. Zheng, Y. Jiang, V. Ladizhansky, L. S. Brown, and H. Liang, ACS Nano **8**, 537 (2014).

8. H.-J. Choi and C. D. Montemagno, Nano Lett. **5**, 2538 (2005).

9. V. Malinova, M. Nallani, W. P. Meier, and E. K. Sinner, FEBS Lett. **586**, 2146 (2012).

10. P. Tanner, P. Baumann, R. Enea, O. Onaca, C. G. Palivan, and W. P. Meier, Acc. Chem. Res. **44**, 1039 (2011).

11. C. Hélix-Nielsen, Anal. Bioanal. Chem. **395**, 697 (2009).

12. Nanyang Technological University, Aquaporin AS, C. Y. Tang, C. Qiu, Y. Zhao, W. Shen, A. Vararattanavech, R. Wang, X. Hu, J. Torres, et al., *Aquaporin based thin film composite membranes*, WIPO (2013).

13. C. Y. Tang, Y. Zhao, R. Wang, C. Hélix-Nielsen, and A. G. Fane, Desalination **308**, 34 (2013).

14. C. Y. Tang, Z. Wang, I. Petrinić, A. G. Fane, and C. Hélix-Nielsen, Desalination **368**, 89 (2015).

15. P. S. Zhong, T.-S. Chung, K. Jeyaseelan, and A. Armugam, J. Membr. Sci. **407-408**, 27 (2012).

16. H. L. Wang, T.-S. Chung, Y. W. Tong, K. Jeyaseelan, A. Armugam, H. H. P. Duong, F. Fu, H. Seah, J. Yang, and M. Hong, J. Membr. Sci. **434**, 130 (2013).

17. M. Antonietti and S. Förster, Adv. Mater. **15**, 1323 (2003).

18. G. Srinivas, D. E. Discher, and M. L. Klein, Nat. Mater. **3**, 638 (2004).

19. G. Srinivas, D. E. Discher, and M. Klein, Nano Lett. **5**, 2343 (2005).

20. P. V. Komarov, I. N. Veselov, and P. G. Khalatur, Chem. Phys. Lett. **605-606**, 22 (2014).

21. M. Kumar, J. Habel, Y.-x. Shen, W. P. Meier, and T. Walz, J. Am. Chem. Soc **134**, 18631 (2012).

22. X. Zhang, P. Tanner, A. Graff, C. G. Palivan, and W. P. Meier, J. Polym. Sci. A Polym. Chem. **50**, 2293 (2012).

23. Y. Won, A. K. Brannan, H. Davis, and F. S. Bates, J. Phys. Chem. B **106**, 3354 (2002).

24. S. Yu, T. Azzam, I. Rouiller, and A. Eisenberg, J. Am. Chem. Soc **131**, 10557 (2009).

25. K. Kita-Tokarczyk, F. Itel, M. Grzelakowski, S. Egli, P. Rossbach, and W. P. Meier, Langmuir **25**, 9847 (2009).

26. M. Xiao, J. Liu, J. Yang, R. Wang, and D. Xie, Soft Matter **9**, 2434 (2013).

27. J. F. Le Meins, O. Sandre, and S. Lecommandoux, Eur. Phys. J. E **34**, 14 (2011).

28. R. Dimova, U. Seifert, B. Pouligny, S. Förster, and H.-G. Döbereiner, Eur. Phys. J. E **7**, 241 (2002).

29. A. Choucair, C. Lavigueur, and A. Eisenberg, Langmuir **20**, 3894 (2004).

30. D. A. Hajduk, M. B. Kossuth, M. A. Hillmyer, and F. S. Bates, J. Phys. Chem. B **102**, 4269 (1998).

31. W. Wang, A. M. McConaghy, L. Tetley, and I. F. Uchegbu, Langmuir **17**, 631 (2001).

32. H. Aranda-Espinoza, H. Bermudez, F. S. Bates, and D. E. Discher, Phys. Rev. Lett. **87**, 208301 (2001).

33. F. Itel, M. Chami, A. Najer, S. Lörcher, D. Wu, I. A. Dinu, and W. P. Meier, Macromolecules **47**, 7588 (2014).

34. D. Wu, M. Spulber, F. Itel, M. Chami, T. Pfohl, C. G. Palivan, and W. P. Meier, Macromolecules **47**, 5060 (2014).

35. O. Terreau, L. Luo, and A. Eisenberg, Langmuir **19**, 5601 (2003).

36. O. Terreau, C. Bartels, and A. Eisenberg, Langmuir **20**, 637 (2004).

37. R. T. Pearson, N. J. Warren, A. L. Lewis, S. P. Armes, and G. Battaglia, Macromolecules **46**, 1400 (2013).

38. H. Shen and A. Eisenberg, J. Phys. Chem. B **103**, 9473 (1999).

39. M. M. Santore, D. E. Discher, Y.-Y. Won, F. S. Bates, and D. A. Hammer, Langmuir **18**, 7299 (2002).

40. S. Rameez, U. Banerjee, J. Fontes, A. Roth, and A. F. Palmer, Macromolecules **45**, 2385 (2012).

41. R. J. R. W. Peters, M. Marguet, S. Marais, M. W. Fraaije, J. C. M. van Hest, and S. Lecommandoux, Angew. Chem. Int. Ed. **53**, 146 (2014).

42. A. Carlsen, N. Glaser, J.-F. Le Meins, and S. Lecommandoux, Langmuir **27**, 4884 (2011).

43. M. Marguet, O. Sandre, and S. Lecommandoux, Langmuir **28**, 2035 (2012).

44. B. M. Discher, H. Bermudez, D. A. Hammer, D. E. Discher, Y.-Y. Won, and F. S. Bates, J. Phys. Chem. B **106**, 2848 (2002).

45. D. E. Discher and A. Eisenberg, Science **297**, 967 (2002).

46. F. He and Y. W. Tong, RSC Adv. **4**, 15304 (2014).

47. S. Li and A. F. Palmer, Macromolecules **38**, 5686 (2005).

48. S. Jain, X. Gong, L. Scriven, and F. S. Bates, Phys. Rev. Lett. **96**, 138304 (2006).

49. S. Jain, M. H. E. Dyrdahl, X. Gong, L. E. Scriven, and F. S. Bates, Macromolecules **41**, 3305 (2008).

50. J. A. Zupancich, F. S. Bates, and M. A. Hillmyer, Biomacromolecules **10**, 1554 (2009).

51. H. Bermudez, A. K. Brannan, D. A. Hammer, F. S. Bates, and D. E. Discher, Macromolecules **35**, 8203 (2002).

52. V. Pata, F. Ahmed, D. E. Discher, and N. Dan, Langmuir **20**, 3888 (2004).

53. K. Davis, T. Lodge, and F. S. Bates, Macromolecules **41**, 8289 (2008).

54. J. J. Lin, J. A. Silas, H. Bermudez, V. T. Milam, F. S. Bates, and D. A. Hammer, Langmuir **20**, 5493 (2004).

55. P. A. Hassan and S. K. Kulshreshtha, J. Colloid Interface Sci. **300**, 744 (2006).

56. S. Förster and E. Krämer, Macromolecules **32**, 2783 (1999).

57. M. A. Hillmyer and F. S. Bates, Macromolecules **29**, 6994 (1996).

58. B. Coldren, R. van Zanten, M. J. Mackel, J. A. Zasadzinski, and H.-T. Jung, Langmuir **19**, 5632 (2003).

59. K. Kita-Tokarczyk and W. P. Meier, Chimia **62**, 820 (2008).

60. G. Mie, Ann. Phys. **330**, 377 (1908).

61. R. Bro and S. De Jong, J. Chemometrics **11**, 393 (1997).

62. B. E. Dahneke, *Measurement of Suspended Particles by Quasi-elastic Light Scattering* (Jon Wiley & Sons, Hoboken, NJ, USA, 1983).

63. B. J. Berne and R. Pecora, *Dynamic light scattering* (Courier Dover Publications, Mineola, NY, USA, 2000).

64. M. L. Carasso, W. N. Rowlands, and R. A. Kennedy, J. Colloid Interface Sci. **174**, 405 (1995).

65. J. Habel, A. Ogbonna, N. Larsen, S. Cherré, S. Kynde, S. R. Midtgaard, K. Kinoshita, S. Krabbe, G. V. Jensen, J. S. Hansen, et al., RSC Adv. **5**, 79924 (2015).

66. L. P. Aggerbeck and T. Gulik-Krzywicki, Methods Enzymol. **128**, 457 (1986).

67. P. Chambon, A. Blanazs, G. Battaglia, and S. P. Armes, Macromolecules **45**, 5081 (2012).

68. L. Ma and A. Eisenberg, Langmuir **25**, 13730 (2009).

69. C. M. Tone, M. P. De Santo, M. G. Buonomenna, G. Golemme, and F. Ciuchi, Soft Matter **8**, 8478 (2012).